Research Article | Vol. 8, No. 2 | 1 Feb 2017 | BIOMEDICAL OPTICS EXPRESS 555

Biomedical Optics EXPRESS

Normalization of compression-induced hemodynamics in patients responding to neoadjuvant chemotherapy monitored by dynamic tomographic optical breast imaging (DTOBI)

AMIR Y. SAJJADI,[1,2,7,8] STEVEN J. ISAKOFF,[3,4,7,9] BIN DENG,[1,2] BHAWANA SINGH,[1,2] CHRISTY M. WANYO,[1] QIANQIAN FANG,[5] MICHELLE C. SPECHT,[3,6] LIDIA SCHAPIRA,[3,4] BEVERLY MOY,[3,4] ADITYA BARDIA,[3,4] DAVID A. BOAS,[1,2] AND STEFAN A. CARP[1,2]

[1]*Optics Division, Athinoula A. Martinos Center for Biomedical Imaging, Massachusetts General Hospital, Charlestown, MA 02129, USA*
[2]*Department of Radiology, Harvard Medical School, Charlestown, MA 02129, USA*
[3]*Massachusetts General Hospital Cancer Center, Boston, MA 02114, USA*
[4]*Department of Medicine, Harvard Medical School, Boston, MA 02114, USA*
[5]*Department of Bioengineering, Northeastern University, Boston, MA 0211, USA*
[6]*Department of Surgery, Harvard Medical School, Boston, MA 02114, USA*
[7]*These authors contributed equally to this work*
[8]*asajjadi@nmr.mgh.harvard.edu*
[9]*sisakoff@mgh.harvard.edu*

Abstract: We characterize novel breast cancer imaging biomarkers for monitoring neoadjuvant chemotherapy (NACT) and predicting outcome. Specifically, we recruited 30 patients for a pilot study in which NACT patients were imaged using dynamic tomographic optical breast imaging (DTOBI) to quantify the hemodynamic changes due to partial mammographic compression. DTOBI scans were obtained pre-treatment (referred to as day 0), as well as 7 and 30 days into therapy on female patients undergoing NACT. We present data for the 13 patients who participated in both day 0 and 7 measurements and had evaluable data, of which 7 also returned for day 30 measurements. We acquired optical images over 2 minutes following 4-8 lbs (18-36 N) of compression. The timecourses of tissue-volume averaged total hemoglobin (HbT), as well as hemoglobin oxygen saturation (SO_2) in the tumor vs. surrounding tissues were compared. Outcome prediction metrics based on the differential behavior in tumor vs. normal areas for responders (>50% reduction in maximum diameter) vs. non-responders were analyzed for statistical significance. At baseline, all patients exhibit an initial decrease followed by delayed recovery in HbT, and SO_2 in the tumor area, in contrast to almost immediate recovery in surrounding tissue. At day 7 and 30, this contrast is maintained in non-responders; however, in responders, the contrast in hemodynamic time-courses between tumor and normal tissue starts decreasing at day 7 and substantially disappears at day 30. At day 30 into NACT, responding tumors demonstrate "normalization" of compression induced hemodynamics vs. surrounding normal tissue whereas non-responding tumors did not. This data suggests that DTOBI imaging biomarkers, which are governed by the interplay between tissue biomechanics and oxygen metabolism, may be suitable for guiding NACT by offering early predictions of treatment outcome.

OCIS codes: (170.2655) Functional monitoring and imaging; (170.3880) Medical and biological imaging; (170.4580) Optical diagnostics for medicine; (170.0170) Medical optics and biotechnology; (170.3890) Medical optics instrumentation.

#273005 http://dx.doi.org/10.1364/BOE.8.000555
Journal © 2017 Received 22 Aug 2016; revised 4 Nov 2016; accepted 5 Dec 2016; published 4 Jan 2017

Biomedical Optics EXPRESS

References and links

1. GLOBOCAN2008, "Estimated cancer Incidence, Mortality, Prevalence and Disability-adjusted life years (DALYs) Worldwide in 2008" (International Agency for Research on Cancer), retrieved October 1, 2013, *http://globocan.iarc.fr/*.
2. N. A. Chatterjee, Y. He, and N. L. Keating, "Racial Differences in Breast Cancer Stage at Diagnosis in the Mammography Era," Am. J. Public Health **103**(1), 170–176 (2013).
3. D. A. Berry, K. A. Cronin, S. K. Plevritis, D. G. Fryback, L. Clarke, M. Zelen, J. S. Mandelblatt, A. Y. Yakovlev, J. D. Habbema, and E. J. Feuer; Cancer Intervention and Surveillance Modeling Network (CISNET) Collaborators, "Effect of screening and adjuvant therapy on mortality from breast cancer," N. Engl. J. Med. **353**(17), 1784–1792 (2005).
4. ACS, "National Cancer Data Base Benchmark Reports," in *http://www.facs.org/cancer/ncdb/publicaccess.html*, (American College of Surgeons, 2013).
5. S. Chia, S. M. Swain, D. R. Byrd, and D. A. Mankoff, "Locally advanced and inflammatory breast cancer," J. Clin. Oncol. **26**(5), 786–790 (2008).
6. N. Wolmark, J. Wang, E. Mamounas, J. Bryant, and B. Fisher, "Preoperative chemotherapy in patients with operable breast cancer: nine-year results from National Surgical Adjuvant Breast and Bowel Project B-18," Journal of the National Cancer Institute. Monographs, 96–102 (2001).
7. J. S. Mieog, J. A. van der Hage, and C. J. van de Velde, "Neoadjuvant chemotherapy for operable breast cancer," Br. J. Surg. **94**(10), 1189–1200 (2007).
8. P. Rastogi, S. J. Anderson, H. D. Bear, C. E. Geyer, M. S. Kahlenberg, A. Robidoux, R. G. Margolese, J. L. Hoehn, V. G. Vogel, S. R. Dakhil, D. Tamkus, K. M. King, E. R. Pajon, M. J. Wright, J. Robert, S. Paik, E. P. Mamounas, and N. Wolmark, "Preoperative chemotherapy: updates of National Surgical Adjuvant Breast and Bowel Project Protocols B-18 and B-27," J. Clin. Oncol. **26**(5), 778–785 (2008).
9. J. A. van der Hage, C. J. van de Velde, J. P. Julien, M. Tubiana-Hulin, C. Vandervelden, and L. Duchateau, "Preoperative chemotherapy in primary operable breast cancer: results from the European Organization for Research and Treatment of Cancer trial 10902," J. Clin. Oncol. **19**(22), 4224–4237 (2001).
10. C. Liedtke, C. Mazouni, K. R. Hess, F. André, A. Tordai, J. A. Mejia, W. F. Symmans, A. M. Gonzalez-Angulo, B. Hennessy, M. Green, M. Cristofanilli, G. N. Hortobagyi, and L. Pusztai, "Response to neoadjuvant therapy and long-term survival in patients with triple-negative breast cancer," J. Clin. Oncol. **26**(8), 1275–1281 (2008).
11. V. Guarneri, K. Broglio, S. W. Kau, M. Cristofanilli, A. U. Buzdar, V. Valero, T. Buchholz, F. Meric, L. Middleton, G. N. Hortobagyi, and A. M. Gonzalez-Angulo, "Prognostic value of pathologic complete response after primary chemotherapy in relation to hormone receptor status and other factors," J. Clin. Oncol. **24**(7), 1037–1044 (2006).
12. P. Cortazar, L. Zhang, M. Untch, K. Mehta, J. P. Costantino, N. Wolmark, H. Bonnefoi, D. Cameron, L. Gianni, P. Valagussa, S. M. Swain, T. Prowell, S. Loibl, D. L. Wickerham, J. Bogaerts, J. Baselga, C. Perou, G. Blumenthal, J. Blohmer, E. P. Mamounas, J. Bergh, V. Semiglazov, R. Justice, H. Eidtmann, S. Paik, M. Piccart, R. Sridhara, P. A. Fasching, L. Slaets, S. Tang, B. Gerber, C. E. Geyer, Jr., R. Pazdur, N. Ditsch, P. Rastogi, W. Eiermann, and G. von Minckwitz, "Pathological complete response and long-term clinical benefit in breast cancer: the CTNeoBC pooled analysis," Lancet **384**(9938), 164–172 (2014).
13. G. von Minckwitz, J. U. Blohmer, S. D. Costa, C. Denkert, H. Eidtmann, W. Eiermann, B. Gerber, C. Hanusch, J. Hilfrich, J. Huober, C. Jackisch, M. Kaufmann, S. Kümmel, S. Paepke, A. Schneeweiss, M. Untch, D. M. Zahm, K. Mehta, and S. Loibl, "Response-Guided Neoadjuvant Chemotherapy for Breast Cancer," J. Clin. Oncol. **31**(29), 3623–3630 (2013).
14. E. Yeh, P. Slanetz, D. B. Kopans, E. Rafferty, D. Georgian-Smith, L. Moy, E. Halpern, R. Moore, I. Kuter, and A. Taghian, "Prospective comparison of mammography, sonography, and MRI in patients undergoing neoadjuvant chemotherapy for palpable breast cancer," AJR Am. J. Roentgenol. **184**(3), 868–877 (2005).
15. A. A. Tardivon, L. Ollivier, C. El Khoury, and F. Thibault, "Monitoring therapeutic efficacy in breast carcinomas," Eur. Radiol. **16**(11), 2549–2558 (2006).
16. K. Wasser, S. K. Klein, C. Fink, H. Junkermann, H. P. Sinn, I. Zuna, M. V. Knopp, and S. Delorme, "Evaluation of neoadjuvant chemotherapeutic response of breast cancer using dynamic MRI with high temporal resolution," Eur. Radiol. **13**(1), 80–87 (2003).
17. A. Hönig, L. Rieger, M. Sutterlin, J. Dietl, and E. F. Solomayer, "Preoperative chemotherapy and endocrine therapy in patients with breast cancer," Clin. Breast Cancer **5**(3), 198–207 (2004).
18. O. J. Stoetzer, D. M. Fersching, C. Salat, O. Steinkohl, C. J. Gabka, U. Hamann, M. Braun, A. M. Feller, V. Heinemann, B. Siegele, D. Nagel, and S. Holdenrieder, "Prediction of response to neoadjuvant chemotherapy in breast cancer patients by circulating apoptotic biomarkers nucleosomes, DNAse, cytokeratin-18 fragments and survivin," Cancer Lett. **336**(1), 140–148 (2013).
19. A. Berriolo-Riedinger, C. Touzery, J. M. Riedinger, M. Toubeau, B. Coudert, L. Arnould, C. Boichot, A. Cochet, P. Fumoleau, and F. Brunotte, "[18F]FDG-PET predicts complete pathological response of breast cancer to neoadjuvant chemotherapy," Eur. J. Nucl. Med. Mol. Imaging **34**(12), 1915–1924 (2007).
20. J. Schwarz-Dose, M. Untch, R. Tiling, S. Sassen, S. Mahner, S. Kahlert, N. Harbeck, A. Lebeau, W. Brenner, M. Schwaiger, F. Jaenicke, and N. Avril, "Monitoring primary systemic therapy of large and locally advanced breast cancer by using sequential positron emission tomography imaging with [18F]fluorodeoxyglucose," J. Clin. Oncol. **27**(4), 535–541 (2008).
21. Y. Yu, Q. Jiang, Y. Miao, J. Li, S. Bao, H. Wang, C. Wu, X. Wang, J. Zhu, Y. Zhong, E. M. Haacke, and J. Hu, "Quantitative analysis of clinical dynamic contrast-enhanced MR imaging for evaluating treatment response in human breast cancer," Radiology **257**(1), 47–55 (2010).

Biomedical Optics EXPRESS

22. H. M. Baek, J. H. Chen, K. Nie, H. J. Yu, S. Bahri, R. S. Mehta, O. Nalcioglu, and M. Y. Su, "Predicting pathologic response to neoadjuvant chemotherapy in breast cancer by using MR imaging and quantitative 1H MR spectroscopy," Radiology **251**(3), 653–662 (2009).
23. U. Sharma, K. K. Danishad, V. Seenu, and N. R. Jagannathan, "Longitudinal study of the assessment by MRI and diffusion-weighted imaging of tumor response in patients with locally advanced breast cancer undergoing neoadjuvant chemotherapy," NMR Biomed. **22**(1), 104–113 (2009).
24. M. D. Pickles, P. Gibbs, M. Lowry, and L. W. Turnbull, "Diffusion changes precede size reduction in neoadjuvant treatment of breast cancer," Magn. Reson. Imaging **24**(7), 843–847 (2006).
25. G. M. McDermott, A. Welch, R. T. Staff, F. J. Gilbert, L. Schweiger, S. I. Semple, T. A. Smith, A. W. Hutcheon, I. D. Miller, I. C. Smith, and S. D. Heys, "Monitoring primary breast cancer throughout chemotherapy using FDG-PET," Breast Cancer Res. Treat. **102**(1), 75–84 (2007).
26. M. L. Marinovich, F. Sardanelli, S. Ciatto, E. Mamounas, M. Brennan, P. Macaskill, L. Irwig, G. von Minckwitz, and N. Houssami, "Early prediction of pathologic response to neoadjuvant therapy in breast cancer: systematic review of the accuracy of MRI," Breast **21**(5), 669–677 (2012).
27. P. J. Bolan, "Magnetic resonance spectroscopy of the breast: current status," Magn. Reson. Imaging Clin. N. Am. **21**(3), 625–639 (2013).
28. R. Choe and T. Durduran, "Diffuse Optical Monitoring of the Neoadjuvant Breast Cancer Therapy," IEEE J. Sel. Top. Quantum Electron. **18**(4), 1367–1386 (2012).
29. F. F. Jöbsis, "Noninvasive, infrared monitoring of cerebral and myocardial oxygen sufficiency and circulatory parameters," Science **198**(4323), 1264–1267 (1977).
30. S. Ueda, D. Roblyer, A. Cerussi, A. Durkin, A. Leproux, Y. Santoro, S. Xu, T. D. O'Sullivan, D. Hsiang, R. Mehta, J. Butler, and B. J. Tromberg, "Baseline tumor oxygen saturation correlates with a pathologic complete response in breast cancer patients undergoing neoadjuvant chemotherapy," Cancer Res. **72**(17), 4318–4328 (2012).
31. A. E. Cerussi, V. W. Tanamai, D. Hsiang, J. Butler, R. S. Mehta, and B. J. Tromberg, "Diffuse optical spectroscopic imaging correlates with final pathological response in breast cancer neoadjuvant chemotherapy," Philos Trans A Math Phys Eng Sci **369**(1955), 4512–4530 (2011).
32. D. Roblyer, S. Ueda, A. Cerussi, W. Tanamai, A. Durkin, R. Mehta, D. Hsiang, J. A. Butler, C. McLaren, W. P. Chen, and B. Tromberg, "Optical imaging of breast cancer oxyhemoglobin flare correlates with neoadjuvant chemotherapy response one day after starting treatment," Proc. Natl. Acad. Sci. U.S.A. **108**(35), 14626–14631 (2011).
33. Q. Zhu, P. A. DeFusco, A. Ricci, Jr., E. B. Cronin, P. U. Hegde, M. Kane, B. Tavakoli, Y. Xu, J. Hart, and S. H. Tannenbaum, "Breast cancer: assessing response to neoadjuvant chemotherapy by using US-guided near-infrared tomography," Radiology **266**(2), 433–442 (2013).
34. O. Falou, H. Soliman, A. Sadeghi-Naini, S. Iradji, S. Lemon-Wong, J. Zubovits, J. Spayne, R. Dent, M. Trudeau, J. F. Boileau, F. C. Wright, M. J. Yaffe, and G. J. Czarnota, "Diffuse optical spectroscopy evaluation of treatment response in women with locally advanced breast cancer receiving neoadjuvant chemotherapy," Transl. Oncol. **5**(4), 238–246 (2012).
35. S. Jiang, B. W. Pogue, C. M. Carpenter, S. P. Poplack, W. A. Wells, C. A. Kogel, J. A. Forero, L. S. Muffly, G. N. Schwartz, K. D. Paulsen, and P. A. Kaufman, "Evaluation of breast tumor response to neoadjuvant chemotherapy with tomographic diffuse optical spectroscopy: case studies of tumor region-of-interest changes," Radiology **252**(2), 551–560 (2009).
36. M. L. Flexman, H. K. Kim, J. E. Gunther, E. A. Lim, M. C. Alvarez, E. Desperito, K. Kalinsky, D. L. Hershman, and A. H. Hielscher, "Optical biomarkers for breast cancer derived from dynamic diffuse optical tomography," J. Biomed. Opt. **18**(9), 096012 (2013).
37. S. Jiang, B. W. Pogue, K. E. Michaelsen, M. Jermyn, M. A. Mastanduno, T. E. Frazee, P. A. Kaufman, and K. D. Paulsen, "Pilot study assessment of dynamic vascular changes in breast cancer with near-infrared tomography from prospectively targeted manipulations of inspired end-tidal partial pressure of oxygen and carbon dioxide," J. Biomed. Opt. **18**(7), 076011 (2013).
38. D. R. Busch, R. Choe, T. Durduran, D. H. Friedman, W. B. Baker, A. D. Maidment, M. A. Rosen, M. D. Schnall, and A. G. Yodh, "Blood Flow Reduction in Breast Tissue due to Mammographic Compression," Acad. Radiol. **21**(2), 151–161 (2014).
39. R. Al Abdi, H. L. Graber, Y. Xu, and R. L. Barbour, "Optomechanical imaging system for breast cancer detection," J. Opt. Soc. Am. A **28**(12), 2473–2493 (2011).
40. M. L. Flexman, M. A. Khalil, R. Al Abdi, H. K. Kim, C. J. Fong, E. Desperito, D. L. Hershman, R. L. Barbour, and A. H. Hielscher, "Digital optical tomography system for dynamic breast imaging," J. Biomed. Opt. **16**(7), 076014 (2011).
41. S. Jiang, B. W. Pogue, K. D. Paulsen, C. Kogel, and S. P. Poplack, "In vivo near-infrared spectral detection of pressure-induced changes in breast tissue," Opt. Lett. **28**(14), 1212–1214 (2003).
42. S. Nioka, S. Wen, J. Zhang, J. Du, X. Intes, Z. Zhao, and B. Chance, "Simulation study of breast tissue hemodynamics during pressure perturbation," Adv. Exp. Med. Biol. **566**, 17–22 (2005).
43. R. X. Xu, B. Qiang, J. J. Mao, and S. P. Povoski, "Development of a handheld near-infrared imager for dynamic characterization of in vivo biological tissue systems," Appl. Opt. **46**(30), 7442–7451 (2007).
44. S. A. Carp, A. Y. Sajjadi, C. M. Wanyo, Q. Fang, M. C. Specht, L. Schapira, B. Moy, A. Bardia, D. A. Boas, and S. J. Isakoff, "Hemodynamic signature of breast cancer under fractional mammographic compression using a dynamic diffuse optical tomography system," Biomed. Opt. Express **4**(12), 2911–2924 (2013).

Biomedical Optics EXPRESS

45. L. S. Fournier, D. Vanel, A. Athanasiou, W. Gatzemeier, I. V. Masuykov, A. R. Padhani, C. Dromain, K. Galetti, R. Sigal, A. Costa, and C. Balleyguier, "Dynamic optical breast imaging: a novel technique to detect and characterize tumor vessels," Eur. J. Radiol. **69**(1), 43–49 (2009).
46. G. J. Zhang, "DOBI Comfortscan System Clinical Effectiveness Evaluation Report" (DOBI Medical International, 2011), retrieved 11/4, 2016, *http://dobiglobal.com/pdfs/DOBIComfortScan_Clinical_Report_2011.pdf*.
47. S. A. Carp, T. Kauffman, Q. Fang, E. Rafferty, R. Moore, D. Kopans, and D. Boas, "Compression-induced changes in the physiological state of the breast as observed through frequency domain photon migration measurements," J. Biomed. Opt. **11**(6), 064016 (2006).
48. S. A. Carp, J. Selb, Q. Fang, R. Moore, D. B. Kopans, E. Rafferty, and D. A. Boas, "Dynamic functional and mechanical response of breast tissue to compression," Opt. Express **16**(20), 16064–16078 (2008).
49. E. P. Mamounas, G. Tang, B. Fisher, S. Paik, S. Shak, J. P. Costantino, D. Watson, C. E. Geyer, Jr., D. L. Wickerham, and N. Wolmark, "Association between the 21-gene recurrence score assay and risk of locoregional recurrence in node-negative, estrogen receptor-positive breast cancer: results from NSABP B-14 and NSABP B-20," J. Clin. Oncol. **28**(10), 1677–1683 (2010).
50. A. Cerussi, D. Hsiang, N. Shah, R. Mehta, A. Durkin, J. Butler, and B. J. Tromberg, "Predicting response to breast cancer neoadjuvant chemotherapy using diffuse optical spectroscopy," Proc. Natl. Acad. Sci. U.S.A. **104**(10), 4014–4019 (2007).
51. Q. Fang, S. A. Carp, J. Selb, G. Boverman, Q. Zhang, D. B. Kopans, R. H. Moore, E. L. Miller, D. H. Brooks, and D. A. Boas, "Combined optical imaging and mammography of the healthy breast: optical contrast derived from breast structure and compression," IEEE Trans. Med. Imaging **28**(1), 30–42 (2009).
52. M. Sridhar and M. F. Insana, "Ultrasonic measurements of breast viscoelasticity," Med. Phys. **34**(12), 4757–4767 (2007).
53. M. Sridhar, C. Pellot-Barakat, and M. F. Insana, "Ultrasonic Mechanical Relaxation imaging," in *2003 Ieee Ultrasonics Symposium Proceedings, **Vols 1 and 2***, D. E. Yuhas and S. C. Schneider, eds. (2003), pp. 929–932.
54. P. Carmeliet and R. K. Jain, "Principles and mechanisms of vessel normalization for cancer and other angiogenic diseases," Nat. Rev. Drug Discov. **10**(6), 417–427 (2011).
55. A. G. Sorensen, T. T. Batchelor, W. T. Zhang, P. J. Chen, P. Yeo, M. Wang, D. Jennings, P. Y. Wen, J. Lahdenranta, M. Ancukiewicz, E. di Tomaso, D. G. Duda, and R. K. Jain, "A "vascular normalization index" as potential mechanistic biomarker to predict survival after a single dose of cediranib in recurrent glioblastoma patients," Cancer Res. **69**(13), 5296–5300 (2009).
56. R. K. Jain, "Normalization of tumor vasculature: an emerging concept in antiangiogenic therapy," Science **307**(5706), 58–62 (2005).
57. O. Falou, A. Sadeghi-Naini, S. Prematilake, E. Sofroni, N. Papanicolau, S. Iradji, Z. Jahedmotlagh, S. Lemon-Wong, J. P. Pignol, E. Rakovitch, J. Zubovits, J. Spayne, R. Dent, M. Trudeau, J. F. Boileau, F. C. Wright, M. J. Yaffe, and G. J. Czarnota, "Evaluation of neoadjuvant chemotherapy response in women with locally advanced breast cancer using ultrasound elastography," Transl. Oncol. **6**(1), 17–24 (2013).

1. Introduction

Breast cancer remains the most common cancer and the leading cause of cancer-related death in women worldwide [1]. While advances in mammographic screening have resulted in a shift to earlier stages at initial diagnosis and a reduction in breast cancer mortality [2, 3], stage III locally advanced breast cancers (LABC) still constitute 9% of newly diagnosed cases in the United States. The incidence of LABC can be as high as 14% in vulnerable populations, such as African American and Hispanic patients [4]. Neoadjuvant chemotherapy (NACT) is standard treatment for LABC patients [5] and is increasingly being used even in patients with earlier stage operable tumors because it can improve outcomes by downstaging the disease and increasing breast conserving surgery rates [6–8]. However, NACT is met with heterogeneous outcomes; although 70-80% of patients unselected for breast cancer subtype demonstrate some degree of response, only 15-25% achieve a pathologic complete response (pCR) [8, 9], which correlates with improved disease free (DFS) and overall survival (OS) [10–12].

These challenges motivate the development of reliable methods for early assessment of tumor response to therapy. Such methods would potentially enable oncologists to switch to alternate therapeutic agents, or simply discontinue ineffective therapy and progress to surgery, limiting unnecessary toxicity. Recently published long-term survival data from the GeparTrio trial (N = 2,072 patients) shows a significant DFS/OS benefit for switching clinical non-responders from docetaxel, doxorubicin, and cyclophosphamide (TAC) to combined vinorelbine and capecitabine (NX) vs. a standard course of TAC (DFS: 0.59 hazard ratio (HR), P = 0.001; OS: 0.79 HR, P = 0.048) [13]. This was achieved despite the use of a heterogeneous combination of clinical examination, x-ray mammography and ultrasound for

Biomedical Optics EXPRESS

assessing the early response, methods known to have limited ability in predicting the pathologic response to chemotherapy [14]. Such data suggests accurate response monitoring may enable significant improvements in NACT outcomes, especially for heterogeneous subtypes, such as triple negative breast cancer (TNBC).

Currently, clinical examination, x-ray mammography, ultrasound, and dynamic contrast enhanced MRI (DCE-MRI) are used to monitor tumor size as a marker of response to treatment, and to assess the volume of residual disease after treatment [15]. However, tumor volume changes manifest themselves later than changes in underlying tumor function, such as vascular density [16], even more so in the case of cytostatic and targeted therapies [17]. While research is being done on the development of circulating biomarkers predictive of therapy response [18], imaging remains the most likely avenue for therapy response guidance in the near future. However, to form early predictions of therapy success, we need imaging methods that are more closely related to tissue function, especially if the distinction between partial and complete pathological response is sought. In this respect, positron emission tomography using 2-deoxy-2-[18^F]Fluoro-D-glucose (^{18}F-FDG PET) has been shown to be able to distinguish eventual pCR after 1 or 2 cycles of chemotherapy [19, 20] based on the amount of reduction in the tumor standardized uptake value (SUV). MRI methods such as pharmacokinetic modeling of DCE-MRI timecourses (sensitive to vascular permeability changes) and proton magnetic resonance spectroscopy (^{1}H-MRS, sensitive to the total concentration of choline compounds (tCho) – assumed to be a marker of proliferation) have also been shown to provide mid-treatment pCR predictions [21, 22]. Diffusion weighted MRI (DW-MRI, sensitive to tumor cellularity and integrity of cell membranes by measuring the water apparent diffusion coefficient (ADC)), has been shown to correlate with the degree of pathological response [23, 24], but no studies to date have demonstrated effective pCR predictions.

Despite these positive results, a number of obstacles remain in the way of routine clinical usage of MRI/PET therapy guidance. FDG-PET requires a sufficiently high initial tumor SUV to be able to observe a significant decrease due to therapy [25], and issues of cost, availability, and allowable radiation exposure restrict its use as a serial monitoring technique. On the other hand, MRI challenges include limited specificity for DCE-MRI [26], and the difficulty of obtaining reliable ^{1}H-MRS data due to high needs for operator skill and MRI hardware performance [27], together with substantial costs and time demands on the patients. In addition, there is currently no consensus on optimal timepoints and quantitative response measures for either MRI or PET methods. Thus, there remains a need to develop alternative imaging methods that address the cost and availability issues of functional MRI/PET while offering similar or better performance.

In this context, near-infrared optical spectroscopy and tomography has emerged over the last decade as an alternative functional imaging method for neoadjuvant therapy monitoring that is relatively low-cost, non-invasive, portable, safe for repeated use, and comparatively simple to operate [28]. Near infrared spectroscopy (NIRS) takes advantage of the low optical absorption of biological tissues for light with a wavelength between approximately 650 and 1000 nm [29]. This low absorption allows several centimeters of tissue penetration, permitting characterization of deep structures. Four main chromophores contribute to optical absorption in the near infrared spectral region: oxy- and deoxy-hemoglobin (HbO, HbR), water and lipids. Using multiple light wavelengths, optical imaging and/or quantitative monitoring of these chromophores gives insight into tissue physiology. The main drawback of optical imaging is the rather low spatial resolution (5-10 mm) caused by high tissue scattering in the near-infrared spectral region. However, this is not a significant concern for NACT monitoring, because tumors treated with NACT are rather large (>2 cm) and have a known location, and the focus is on quantification of tissue functional parameters (e.g. Hb concentration) rather than tumor size. Two recent NIRS studies have reported a statistically significant difference between patients that achieved pCR vs. non pCR, with respect to the pre-treatment tumor hemoglobin oxygen saturation SO_2 [30] and with respect to the reduction in HbR and a tissue optical index defined as (HbR x water / lipid) [31]. Several other studies

Biomedical Optics EXPRESS

have shown there is an HbO "flare" in responders immediately after the first dose of chemotherapy [32]. Further, high pre-treatment total hemoglobin (HbT = HbO + HbR) correlates with complete or near complete pathological response [33] and reductions in HbT/ HbO/HbR early during therapy predict greater than 50% eventual tumor shrinkage [33–35].

Dynamic tomographic optical breast imaging (DTOBI) is a novel technique that provides quantitative images of the variations in tissue chromophore concentration during external stimuli and can be used to develop novel imaging biomarkers for breast cancer detection and chemotherapy monitoring. Both gas inhalation/breath-holding [36, 37] and external mechanical stimuli [38–46] have been proposed to develop novel imaging biomarkers of breast cancer. In particular, our group has obtained promising initial results by dynamically imaging the breast tissue response to fractional mammographic compression [47, 48].Tissue viscoelastic relaxation during the compression period leads to a slow reduction in the compression force and reveals biomechanical and metabolic differences between normal and lesion tissue. Using this method, we have shown that there is a significant difference in the hemodynamic response to compression between the tumor area and the surrounding normal tissue in a group of seventeen breast cancer patients [44].

Here we evaluate whether monitoring hemodynamic biomarkers such as variations in the compression induced changes in tissue hemoglobin concentration and oxygen saturation in the tumor area versus the rest of the breast over the first few weeks of therapy can provide predictive information for therapy outcome. We report results from a group of 13 patients with early stage breast cancer receiving neoadjuvant chemotherapy who were evaluated using the DTOBI system pre-treatment, at day 7 and, for 7 of them, at day 30 into treatment.

2. Methods

2.1. Dynamic tomographic optical breast imaging (DTOBI) instrumentation

The DTOBI system (Fig. 1) consists of a high temporal resolution, hybrid continuous wave/frequency domain transmission mode diffuse optical tomography system. The optical instrumentation is integrated into a compression setup also equipped with a Tekscan I-Scan pressure mapping system [44]. The frequency domain component consists of an ISS Imagent (model 96208, ISS Inc., Champaign, IL). Eight time-multiplexed laser diodes at 635, 670, 690, 752, 758, 782, 810 and 830 nm modulated at 110 MHz inject light in the breast at a single central location near the chest wall using an optical fiber bundle. Three red-enhanced photomultiplier tube detectors (Hamamatsu R928 PMT) collect the back scattered light through 2.5 mm optical fiber bundles. The amplitude and phase parameters are extracted by in-phase/quadrature (I/Q) demodulation. The frequency modulated system provides absolute optical properties and is used to obtain the baseline breast bulk hemoglobin concentration that forms the initial homogeneous guess for the 3D tomographic reconstruction based on continuous wave measurements. The continuous wave component consists of a TechEn CW6 imager augmented by a Supplemental Source Device (SSD) (TechEn Inc., Milford, MA). The CW6 offers 32 lasers split equally among 690 and 830 nm as well as 32 avalanche photodiode (APD) detectors. The lasers are modulated at 32 individual frequencies between ~6-12 kHz allowing full simultaneous detection [49]. The SSD adds 32 lasers at additional wavelengths (10 at 780, 11 at 808 and 11 at 850 nm) with each laser sharing a modulation frequency with a corresponding laser in the main CW6 box. Main/supplemental laser sources were illuminated in an interleaved fashion, switching once per second. Even in conjunction with the SSD, the system is able to record all 2048 source-detectors pairs at over 10 Hz, while maintaining high signal-to-noise ratio (>90dB) and linear dynamic range (>60dB). Since expected breast

Biomedical Optics EXPRESS

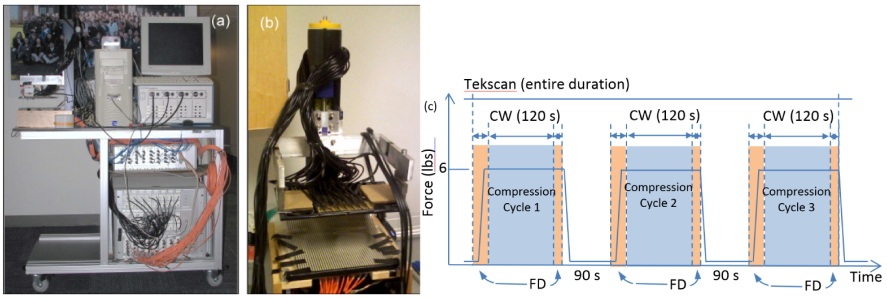

Fig. 1. a) DTOBI Instrument mounted on a mobile cart; b) detail of breast compression probe before cart mounting – the CW sources, all FD fibers and the Tekscan mat are mounted on the lower plate, while the upper, mobile plate carries the CW detector fiber bundles and is attached to the translation mechanism through 2 force gauges. c) Schematic of measurement protocol: three compression cycles (about 26 N or 6 lbs), each beginning with FD recording during the compression and for 2 seconds after, followed by a 2 minute CW recording and another 5 second FD acquisition before the compression was released. The cycles were separated by a 90 second no-compression period (the patient's breast remained in place).

hemodynamics are relatively slow, we averaged the CW data into 2 second windows for improved signal quality. As described below, the Tekscan system further provides a pressure map used to determine the location of the breast with respect to the optical fibers.

2.2 DTOBI measurement procedure

A full description of the experimental setup has been previously published by our group [44]. In summary, the breast is placed between two horizontal parallel plates (equivalent to mammographic craniocaudal (CC) compression), which apply a repeated step compression/release to the breast. The 64 CW source fibers, as well as the FD-NIRS source and three detection bundles (FD source-detectors separations of 1.12, 1.68, 2.24 cm) are inserted in the lower plate, while 30 2.5 mm detector fiber bundles with a 90 degree bent end are mounted into the upper plate to collect light transmitted through the breast and deliver it to the CW detectors. Both the upper and the lower fiber arrays cover an approximately 12x8 cm half elliptical area. The FD source power at the probe is ~2mW, while the CW source fibers deliver ~10 mW. A pressure mapping system (Tekscan I-Scan) with a Tekscan 5250 flat 10"X10" 44x44 element sensor is mounted on the lower fixed plate, and is used to monitor the breast contact patch and spatial distribution of forces during the optical measurements. Fibers in the lower plate are aligned with the transparent windows between the Tekscan sensor rows and columns to allow simultaneous optical imaging and pressure monitoring. As described in detail in reference [38], data is acquired continuously, and operation is controlled by a personal computer running custom software that ensures synchronization of the various optical and mechanical components. Figure 1(a) shows the dynamic optical imaging setup as mounted on a cart that can be wheeled into an examination room, while Fig. 1(b) offers a detail view of the compression and fiber probe sub-assembly. Figure 1(c) illustrates the compression/release protocol and the timing of data acquisition by each optical sub-system. Each breast is scanned in turn and three compression cycles are executed. The FD acquisition is active while the upper plate moves down to apply compression and for the first 2 seconds of the steady compression period, followed by a 2 minute CW acquisition and a final 5 second FD measurement before compression is released. The breast tissue is allowed to relax for 90 second between repeated compressions.

2.3 Therapy monitoring pilot clinical trial protocol

All measurements were conducted under a protocol approved by the Dana Farber/Harvard Cancer Center Institutional Review Board (IRB) and registered in the national clinical trials registry (NCT00783757). All patients involved in the study signed an informed consent form including consent to participate in the study and to publish the anonymized data. Optical

Biomedical Optics EXPRESS

assessment of the HbO, HbR, HbT and SO_2 response to compression at pre-treatment, day 7, and optionally at day 30 and every other cycle during treatment was performed. The patients were women between 29 to 73 years old (median 45 years old) with documented invasive breast cancer. Candidates with breast implants, open wounds on the breast, or breast biopsies within the previous 10 days were excluded. The tumor size ranged from 1.2 to 5.7 cm, with an average of 3.0 cm and a standard deviation of 1.2 cm. Optional scans were also offered during days 2-6 of first cycle seeking to obtain finer grained information but logistical concerns limited subject interest in these scans.

The response to treatment was assessed based on the reduction in the longest lesion diameter between size seen in the pre-treatment imaging scans and the size reported in the final pathology report after surgery. Following the approach of Cerussi et al. [50], we considered a 50% reduction as the threshold for calling a subject a responder. We also recorded pathological complete responses and near-complete responses (>95% reduction) as well, but since we did not achieve statistical significance with respect to these levels of response, we focused our analysis on the responder/non-responder dichotomy defined above.

2.4 Optical image reconstruction and analysis procedures

We use finite element modeling of light propagation in tissue, on a 3D mesh generated from breast contact pressure image. A dual-mesh scheme, a forward denser mesh for diffusion modeling and a separate coarser reconstruction mesh to represent the medium optical properties were used for improved computation efficiency. Hemoglobin concentration values are reconstructed by solving a regularized nonlinear optimization problem using 9 Gauss-Newton iterations [51]. Since the frequency domain measurements are done at a single location, and there are unavoidable shifts of the breasts between measurement sessions, we only used the frequency domain-derived absolute optical properties to provide an approximate baseline for the calculation of the starting hemoglobin oxygen saturation, baseline that is needed for scaling SO_2 values even when only changes are monitored. The rest of our image processing and analysis was based on relative reconstructions derived from the evolution of the CW optical signals during the measurement period.

To quantify tumor and normal tissue properties, we used information from both clinical MRI/x-ray scans and optical image features to define corresponding regions of interest (ROIs), as described in detail in Ref [44]. The shape and size of these ROIs were kept the same for all patient visits, but their absolute location was adjusted to maintain their relationship to the breast boundary as derived from the Tekscan pressure map.

2.5 Statistical analysis

Each patient had a pre-treatment scan, as well as a day 7 and an optional day 30 scan using the DTOBI system. We monitored the tumor vs. normal differential hemodynamic compression response at these three treatment points during therapy and we correlated our measurements to the degree of response. As described above, we used a binary classification of responders (>50% reduction in tumor diameter) and non-responders (<50% reduction in tumor diameter).

In the previous study, we showed that at day 0 (pre-treatment scan), there are differences in hemodynamic properties between tumor region and the surrounding healthy tissue during dynamic compression of the tissue [44] and these differences are statistically significant. In order to find out if monitoring these differences over the course of NACT can help in differentiating the responders vs. non-responders to the NACT, we executed the same protocol to monitor the changes in hemodynamic properties at day 7 and 30 into the NACT. We then compared the compression response of the two independent hemodynamic parameters, HbT and SO_2, between the responder and non-responder groups. We used a two-tailed, paired, t-test between the corresponding values of all optical parameters in the tumor and normal ROIs across the responder and non-responder groups (normality of the data at the 95% confidence level was verified using the Jarque-Bera test as implemented by the Matlab *jbtest* function). The means of hemodynamic parameters (ΔHbT and ΔSO_2) between normal

Biomedical Optics EXPRESS

and tumor region of the breast were tested at different time points of each cycle between responders and non-responders. The t-test was also performed on T-N metric, which is the difference in a given hemodynamic parameter between the tumor and normal region and is calculated at all treatment time points, i.e. day 0, day 7 and day 30 through NACT. Statistical comparisons were made using paired two-tailed t-tests at 0.05 level of significance.

3. Results

Of 30 total patients accrued, 17 subjects were not included for the following reasons: Measurements taken on the first three subjects could not be used because of an error in the data acquisition software that corrupted the data; 1 could not tolerate the compression, 2 did not come back for follow-up scans; 4 subjects had diffuse, multi-focal or excessively large lesions (not possible to establish a healthy tissue reference); and 7 for instrumentation related reasons (tumor not in the field of view in 3 cases, excessive alignment error between scans in one case, and data quality issues in 3 cases). Here we report results from the remaining 13 subjects, 7 of whom also came back for day 30 scans. Table 1 shows the patient demographic information, treatment data, and their degree of response to chemotherapy (assessed post-treatment based on the pathology report).

Table 1. Patient demographic and treatment data.

Patient No.	Tumor side	Age	Menopausal Status	Lesion size (cm)	Tumor Subtypes	NAC Treatment	Degree of Shrinkage	Response Category
5	L	36	pre	3.6	ER + ,PR + ,HER2 +	Paclitaxel/Herceptin Lapatinib	11%	NR
6	R	60	post	2.6	ER-,PR- ,HER2 +	Paclitaxel/trastuzumab	~96%	Near pCR
9	L	44	pre	1.8	ER + ,PR + ,HER2 +	Paclitaxel/trastuzumab lapatinib	77%	PR
11	R	34	pre	3.0	ER + ,PR + ,HER2-	Paclitaxel/bevacizumab doxorubicin/ cyclophosphamide	26%	NR
16	R	38	pre	4.8	ER-,PR- ,HER2-	Paclitaxel/carbo/avastin- doxorubicin/ cyclophosphamide	46%	NR
17	R	41	pre	5.0	ER + ,PR- ,HER2 +	Paclitaxel/trastuzumab/ lapatinib	100%	pCR
19	L	56	post	1.3	ER-,PR- ,HER2 +	Paclitaxel/Herceptin	100%	pCR
22	R	29	pre	2.2	ER-,PR- ,HER2-	Cisplatin/paclitaxel/novel PI3K pathway inhibitor	100%	pCR
23	R	52	pre	5.7	ER-,PR- ,HER2-	Pactilaxel/Cisplatin /rad001	44%	NR
25	L	65	post	1.6	ER + ,PR + ,HER2-	Dose dense doxorubicin/ cyclophosphamide-paclitaxel	19%	NR
26	R	73	post	3.2	ER-,PR- ,HER2-	Dose dense doxorubicin/ cyclophosphamide-paclitaxel	–6%	NR
27	L	39	pre	3.0	ER + ,PR + ,HER2-	Doxorubicin/ cyclophosphamide	–96%	NR
30	R	41	pre	3.7	ER-,PR- ,HER2-	Dose dense doxorubicin/ cyclophosphamide-paclitaxel	69%	PR

pCR: pathologic complete response; near pCR: nearly complete pathologic response (>95% shrinkage) PR: partial response (>50% shrinkage) – pCR, near pCR and PR form the responders group; NR: no response (<50% shrinkage).

Biomedical Optics EXPRESS

In Fig. 2, the measurement of force and corresponding changes in total hemoglobin concentration (ΔHbT) and hemoglobin oxygen saturation (ΔSO_2) are presented for one of the patients at the baseline measurement (day 0). There is a clear difference in time courses of ΔHbT and ΔSO_2 during compression between tumor (T) and normal (N) tissue at day 0. The

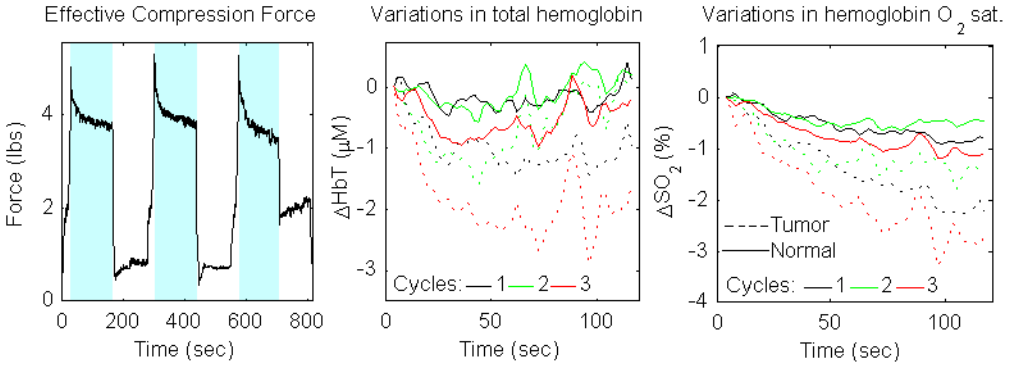

Fig. 2. a) strain gauge force data for the entire measurement on the tumor breast; blue areas highlight the three main compression periods; b,c) HbT/SO_2 variation vs. initial state for the tumor (solid) and normal (dashed) ROIs over the three compression cycles (black, green, red for cycles 1, 2, and 3, respectively)

tumor ROI timecourse is shown as dotted lines (colors indicate the compression cycle), while the normal ROI is shown as solid lines. Although there is significant variation among the compression cycles, in all cases the tumor ROI shows a notable HbT decrease followed by a limited blood volume recovery, whereas the normal ROI has a notable increasing trend from 30 to 120 sec. For SO_2 the differential relationship is similar; while both ROIs show a decrease, a stronger decrease is observed in the tumor area. Figure 2 shows that optical measurements can detect the difference in the compression induced variation of hemodynamic parameters (HbT and SO_2) in tumor vs. normal tissue.

Group averaged changes in HbT and SO_2 in the tumor (blue lines) and normal tissue (red lines) prior to treatment (baseline) and during the treatment (day 7 and day 30) are presented in Figs. 3 and 4, respectively. Based on the differential compression induced changes in HbT and SO_2, the contrast between normal (N) and tumor (T) increases somewhat at day 7 and more noticeably at day 30 in non-responders to NACT. However, in responders, this contrast between tumor and normal tissue decreases during the therapy (partially at day 7) and almost completely disappears by day 30. ΔSO_2 shows a similar trend between responders and non-responders during the course of NACT. Recordings across the three compression cycles are substantially similar.

ROI average values were compared between the non-responder and responder groups at three levels. First, we compared the compression-induced change in both HbT and SO_2 in tumor and normal tissues, respectively, between groups. Next we computed the differential change in tumor vs. normal tissue and compared these differences between groups. Finally, we further computed the variation in the tumor vs. normal differential compression response at day 7 and day 30 vs. pre-treatment, respectively as a measure of the response to therapy. We looked at these metrics at three timepoints during the compression period (t = 30, 60, and 90s) and across the three repetitions of the compression procedure acquired on each measurement day.

Tables 2 and 3 summarize the *p*-values resulting from the t-tests of statistical significance of the differences in the three types of metrics described above between the responder and non-responder groups (note that the results for day 0 and day 7 are based on 13 patients, of which 7 are non-responders and 6 are responders, while the results for day 30 are based on 7 patients, 3 of which are non-responders and 4 of which are responders).

Biomedical Optics EXPRESS

As suggested by Fig. 3 and detailed in Table 2, at day 30, the amounts of compression induced changes in HbT in the tumor areas are significantly smaller in responders vs. non-responders for the 2nd and 3rd compression cycles at all timepoints (t = 30, 60, and 90s), as well as at the midpoint (t = 60s) of the first compression cycle. Similar characteristics are noted for the changes in SO_2 in the tumor areas. Additionally, compression induced changes in SO_2

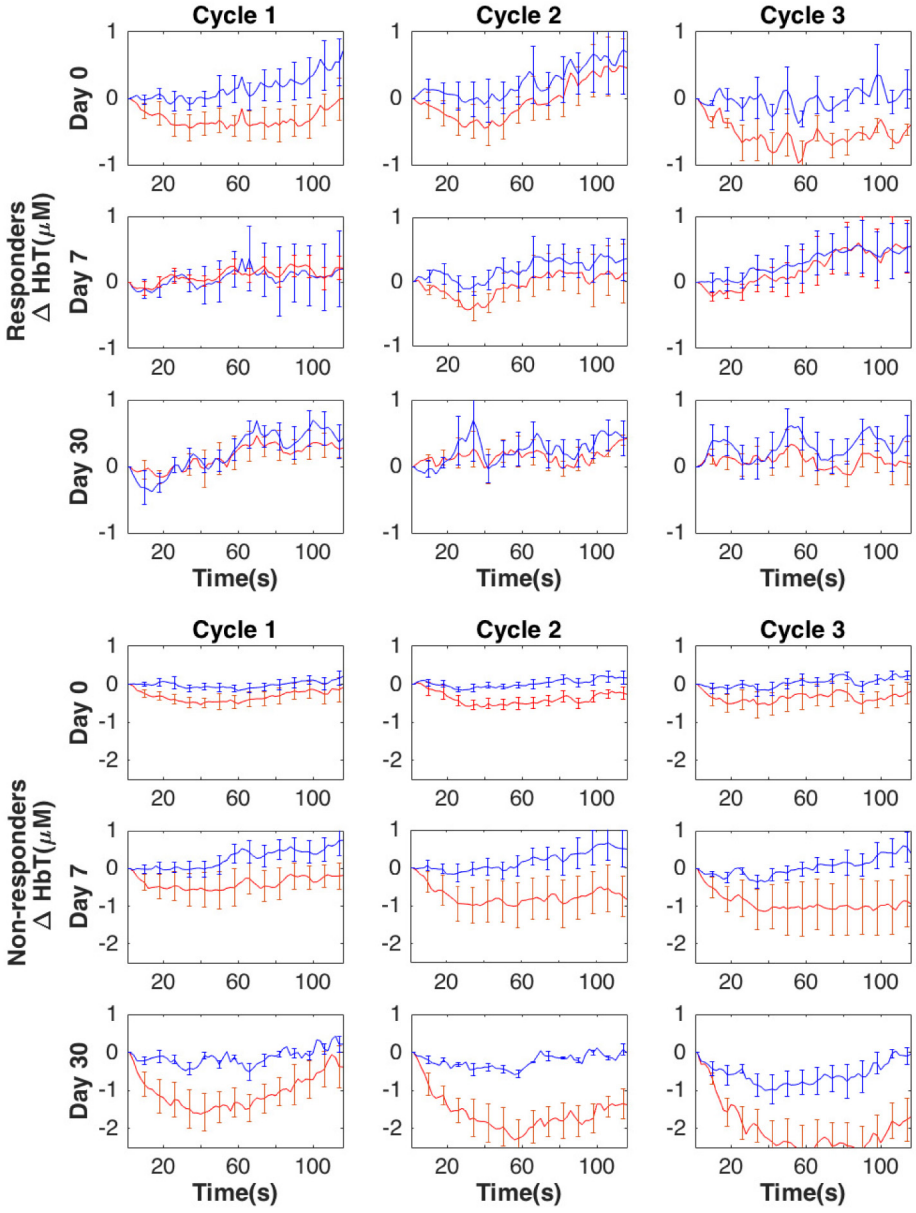

Fig. 3. Group averaged compression induced changes in ΔHbT (μM) for responders and non-responders, respectively, within the tumor (red lines) and normal (blue lines) regions of the breast due to compression over the course of NACT (13 subjects for day 0 and day 7, and 7 subjects for day 30). Error bars show standard error.

Biomedical Optics EXPRESS

in the healthy tissue are significantly larger at the pre-treatment scan during the late (t = 60 and 90s) 2nd and all of the 3rd compression cycle for the responders vs. non-responders.

Proceeding with the analysis, Table 3 shows the statistical analysis of the correlation of the differential compression response between tumor and normal areas. We note that at day 30, due to the apparent "normalization" of the tumor compression response, the tumor vs. normal difference in the HbT compression response is significantly smaller in the responders vs. non-responders for the middle (t = 60 s) of the 2nd and all of the 3rd compression cycle. Further, the same characteristics are seen for the middle and late 3rd compression cycle at day

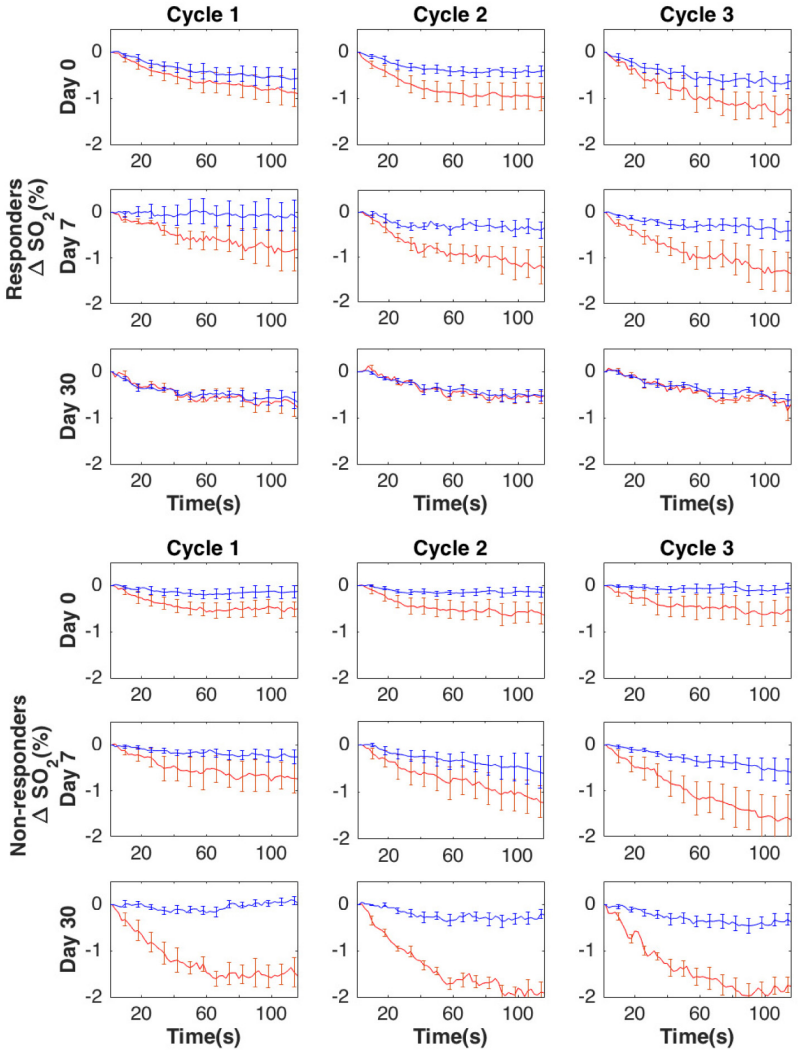

Fig. 4. Group averaged compression induced changes in ΔSO_2 (μM) for responders and non-responders, respectively, within the tumor (red lines) and normal (blue lines) regions of the breast due to compression over the course of NACT (13 subjects for day 0 and day 7, and 7 subjects for day 30). Error bars show standard error.

7 with near significance. SO_2 metrics behave similarly to HbT metrics, with the differences between tumor and normal tissues being significantly smaller at day 30 for the responders vs. non-responders, reaching statistical significance for all cycles and timepoints except early (t = 30 s) in the 1st cycle.

Biomedical Optics EXPRESS

Table 2. *P*-values of t-test of the ΔHbT and ΔSO_2 during compression compared between responders and non-responders. (T = Tumor tissue, N = Normal tissue)

ΔHbT	DAY 0						DAY 7						DAY 30					
	Cycle 1		Cycle 2		Cycle 3		Cycle 1		Cycle 2		Cycle 3		Cycle 1		Cycle 2		Cycle 3	
	T	N	T	N	T	N	T	N	T	N	T	N	T	N	T	N	T	N
30 s	0.50	0.91	0.51	0.70	0.76	0.68	0.16	0.75	0.66	0.40	0.15	0.26	0.15	0.38	**<0.01**	0.27	**<0.01**	0.32
60 s	0.37	0.43	0.34	0.61	0.45	0.19	0.36	0.38	0.44	0.52	0.23	1.00	**0.02**	0.14	**<0.01**	0.18	**0.01**	0.20
90 s	0.82	0.86	0.12	0.47	0.86	0.80	0.57	0.47	0.61	0.45	0.21	0.88	0.39	0.69	**<0.01**	0.41	**<0.01**	0.23
ΔSO_2	DAY 0						DAY 7						DAY 30					
	Cycle 1		Cycle 2		Cycle 3		Cycle 1		Cycle 2		Cycle 3		Cycle 1		Cycle 2		Cycle 3	
	T	N	T	N	T	N	T	N	T	N	T	N	T	N	T	N	T	N
30 s	0.56	0.15	0.27	0.09	0.24	**0.03**	0.73	0.73	0.66	0.43	0.83	0.45	0.22	0.07	**<0.01**	0.36	**<0.01**	0.57
60 s	0.51	0.18	0.20	**0.02**	0.13	**0.02**	0.97	0.67	0.56	0.75	0.88	0.96	0.08	**0.05**	**<0.01**	0.51	**0.05**	0.71
90 s	0.32	0.11	0.28	**0.05**	0.11	**0.02**	0.85	0.73	0.80	0.82	0.83	0.79	0.25	**0.02**	**<0.01**	0.34	**0.04**	0.80

Table 3. *P*-values of t-test on the differences in ΔHbT and ΔSO_2 during compression between tumor and normal areas in the same breast in responders vs. non-responders across timepoints, compression cycles and treatment points.

ΔHbT	DAY 0			DAY 7			DAY 30		
	Cycle 1	Cycle 2	Cycle 3	Cycle 1	Cycle 2	Cycle 3	Cycle 1	Cycle 2	Cycle 3
	T-N	T-N	T-N	T-N	T-N	T-N	T-N	T-N	T-N
30 s	0.50	0.65	1.00	0.12	0.12	0.45	0.20	0.12	**0.03**
60 s	0.93	0.47	0.94	0.08	0.09	**0.05**	0.22	**0.02**	**0.03**
90 s	0.68	0.15	0.97	0.17	0.15	**0.05**	0.45	0.07	**0.03**
ΔSO2	DAY 0			DAY 7			DAY 30		
	Cycle 1	Cycle 2	Cycle 3	Cycle 1	Cycle 2	Cycle 3	Cycle 1	Cycle 2	Cycle 3
	T-N	T-N	T-N	T-N	T-N	T-N	T-N	T-N	T-N
30 s	0.67	0.78	0.97	0.90	0.90	0.99	0.07	**<0.01**	**<0.01**
60 s	0.63	0.76	0.89	0.68	0.60	0.76	**0.03**	**<0.01**	**0.01**
90 s	0.66	0.83	0.83	0.59	0.70	0.79	**0.05**	**<0.01**	**<0.01**

To assess the predictive performance of the compression response metrics, we developed a simple classification scheme based on the amount of change due to compression in the tumor and normal tissues, respectively, as well as based on the difference in compression response between tumor and normal tissues. Tables 4 and 5 report the areas under the receiver operating characteristic curves (ROC) for these predictions. It is generally seen that by day 30 responders can be differentiated from non-responders quite well using either HbT or SO_2 based metrics. More importantly, even at day 7, the eventual response to therapy can be predicted based on the differential tumor vs. normal HbT response for the later timepoints (60 and 90s) with sensitivities and specificities as good as 86%, 71%, 86% and 67%, 67%, 100%, respectively across compression cycles at 60s (or 90s), 60s, and 90s, respectively. The ROC curves for these best case predictions are shown in Fig. 5.

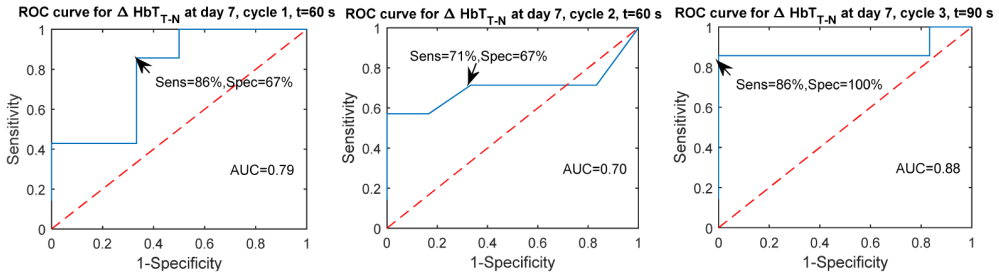

Fig. 5. Receiver Operating Characteristic (ROC) curves for predicting whether a patient will be a responder or non-responder based on the differential change in HbT between the tumor and normal areas at day 7, for t = 60 s, cycle 1, t = 60 s, cycle 2 and t = 90 s, cycle 3.

Biomedical Optics EXPRESS

4. Discussion

The group averaged time courses presented in Figs. 3 and 4 illustrate the compression-induced changes in total hemoglobin and hemoglobin oxygen saturation. The contrast initially present in the tumor vs. normal tissue behavior lessens/disappears in responders, but is maintained in non-responders. These results suggest that dynamic optical measurements can detect chemotherapy-induced differences in the compression-induced variation of hemodynamic parameters (HbT and SO_2) in tumors and normal tissue. Of note, generally better results are seen for the 2nd and 3rd compression cycle, indicating some level of tissue "pre-conditioning" is needed for reliable measurements.

Table 4. Areas under the ROC curve (AUC) for predicting response vs. non-response using ΔHbT and ΔSO_2 change thresholds during compression. (T = Tumor tissue, N = Normal tissue). AUC>0.75 highlighted in bold.

ΔHbT	DAY 0						DAY 7						DAY 30					
	Cycle 1		Cycle 2		Cycle 3		Cycle 1		Cycle 2		Cycle 3		Cycle 1		Cycle 2		Cycle 3	
	T	N	T	N	T	N	T	N	T	N	T	N	T	N	T	N	T	N
30 s	0.60	0.55	0.55	0.52	0.29	0.43	0.64	0.52	0.50	0.43	0.70	0.71	**0.92**	**0.75**	**1.00**	**0.75**	**1.00**	0.67
60 s	0.63	0.67	0.64	0.45	0.33	0.31	0.64	0.39	0.62	0.51	0.67	0.57	**1.00**	**0.83**	**1.00**	**0.83**	**1.00**	**0.83**
90 s	0.40	0.56	**0.81**	0.60	0.43	0.48	0.60	0.40	0.55	0.51	0.70	0.60	**0.75**	0.58	**1.00**	**0.75**	**1.00**	**0.83**

ΔSO_2	DAY 0						DAY 7						DAY 30					
	Cycle 1		Cycle 2		Cycle 3		Cycle 1		Cycle 2		Cycle 3		Cycle 1		Cycle 2		Cycle 3	
	T	N	T	N	T	N	T	N	T	N	T	N	T	N	T	N	T	N
30 s	0.40	0.29	0.30	0.24	0.29	0.15	0.42	0.43	0.33	0.31	0.40	0.31	**0.83**	0.08	**1.00**	0.25	**1.00**	0.42
60 s	0.44	0.36	0.27	0.12	0.27	0.14	0.42	0.38	0.33	0.35	0.57	0.50	**0.92**	0.00	**1.00**	0.25	**1.00**	0.50
90 s	0.43	0.27	0.31	0.19	0.29	0.10	0.40	0.43	0.38	0.45	0.54	0.62	**0.83**	0.00	**1.00**	0.21	**1.00**	0.46

Table 5. Areas under the ROC curve (AUC) for predicting response vs. non-response using the differences in ΔHbT and ΔSO_2 during compression between tumor and normal areas in the same breast. AUC>0.75 highlighted in bold.

ΔHbT	DAY 0			DAY 7			DAY 30		
	Cycle 1	Cycle 2	Cycle 3	Cycle 1	Cycle 2	Cycle 3	Cycle 1	Cycle 2	Cycle 3
	T-N	T-N	T-N	T-N	T-N	T-N	T-N	T-N	T-N
30 s	0.60	0.52	0.40	0.73	0.60	0.60	**0.75**	**0.92**	**1.00**
60 s	0.56	0.61	0.42	**0.79**	0.70	**0.77**	**0.83**	**1.00**	**1.00**
90 s	0.57	0.74	0.50	0.73	0.73	**0.88**	**0.75**	**0.96**	**1.00**
ΔSO_2	**DAY 0**			**DAY 7**			**DAY 30**		
	Cycle 1	Cycle 2	Cycle 3	Cycle 1	Cycle 2	Cycle 3	Cycle 1	Cycle 2	Cycle 3
	T-N	T-N	T-N	T-N	T-N	T-N	T-N	T-N	T-N
30 s	0.44	0.37	0.43	0.30	0.31	0.36	**0.92**	**1.00**	**1.00**
60 s	0.52	0.37	0.45	0.29	0.36	0.44	**1.00**	**1.00**	**1.00**
90 s	0.52	0.40	0.43	0.29	0.30	0.43	**1.00**	**1.00**	**1.00**

The disparity in tumor vs. normal compression response may be driven by the increased stiffness and longer viscoelastic relaxation time of the tumor tissue [52, 53]. As we hold the breast under compression, the stiffer tumor may be bearing a disproportionate amount of the load, "shielding" the normal surrounding tissue. The convergence of the compression response $\Delta HbT/\Delta SO_2$ time-courses between tumor and normal areas at day 7 and even more so at day 30 may be related to the "normalization" of the tumor that has been observed at the microscopic level [54–56]. Further, evaluation of NACT using ultrasound elastography in 15 patients with locally advanced breast cancer showed that as tumors begin to respond to the NACT, their structure and biomechanical properties start to change and become less stiff in responding patients [57].

Biomedical Optics EXPRESS

Our qualitative observations are partially reflected by the results of the statistical analysis. We note the statistically significant difference in compression response of the tumor tissue developing by day 30, as well as the statistically significant decrease in the difference between the behavior of tumor and normal tissue from the same breast for responders also seen by day 30. However, these results did not hold up when the patients were classified in complete vs. less than complete responders. These data suggest that a follow-up study with a larger sample size and perhaps additional intermediate time-points, such as day 14 is warranted to explore the full potential of this technique.

This study experienced several limitations, such as the pilot nature, the small number of patients who allowed the optional Day 30 scan, the heterogeneity of the chemotherapy regimens used, the heterogeneity of tumor subtypes with a preponderance of HER2 positive lesions, that often have better responses to neoadjuvant therapy than other subtypes, and the binary cut off of 50% shrinkage as the responder/non-responder definition. We should note that there may be more clinically meaningful predictive pathological systems to determine response than the 50% shrinkage used here. Among these are achieving pathological complete response vs. not achieving it, or achieving a final residual cancer burden (RCB) of 0/1 vs. 2/3. Future studies will include focusing on patients with more homogenous subtypes and who receive more consistent homogeneous treatments.

Despite limited statistical significance, some predictive ability appears to have been achieved, thus the results of this pilot study are encouraging and suggest dynamic optical imaging can be a useful addition to the range of optical breast imaging techniques. Static imaging techniques that are well validated in the field could be combined with compression response metrics derived from DTOBI data to offer optical imaging tools for monitoring the treatment and predicting the therapy outcome during the early stages of NACT.

5. Conclusion

These initial results suggest that dynamic optical breast imaging can detect changes due to treatment and have predictive value for the treatment outcome. DTOBI can show the difference in hemodynamic response to compression between tumor and normal tissue and demonstrates the feasibility of using dynamic optical breast tomography for neoadjuvant chemotherapy monitoring. Results in a small cohort of 13 patients indicate that the difference in tumor vs. normal response to compression remains largely unchanged in non-responders, while tumor tissue response converges towards normal tissue in responders. Dynamic optical breast imaging may thus, in conjunction with more established static optical imaging techniques, become a convenient, non-invasive and portable tool for chemotherapy monitoring and outcome prediction.

Acknowledgments

This work was supported by NIH grants R00EB011889, R01CA142575, R01CA187595 and the Susan G. Komen for the Cure Foundation grant KG200021. The authors would like to thank Ms. Nancy Nagda for coordinating patient scheduling, the staff of the MGH Center for Breast Cancer for their support, and the patients who participated in this project.